JOURNAL OF MATERIALS SCIENCE 16 (1981) 1029–1038

Quantitative fractography of WC–Co cermets by Auger spectroscopy

R. K. VISWANADHAM, T. S. SUN*, E. F. DRAKE, J. A. PECK
Materials Research, Reed Rock Bit, PO Box 2119, Houston, Texas 77001, USA and
**Martin Marietta Laboratories, 1450 South Rolling Road, Baltimore, Maryland 21227, USA*

A general procedure has been developed to determine the area fraction occupied by the binder on the fracture surfaces of cemented carbides. The area fraction of binder on the fracture surface was obtained from the relative peak-to-peak height ratios of elements in the binder and the carbide content was measured by Auger spectroscopy on the fracture surface and an adjacent polished section and the volume fraction of binder present in the cermet. This procedure was employed to determine the area fraction of binder on the fracture surfaces of WC–Co cermets with different binder contents and carbide grain sizes. The average binder mean free path and the area fraction of binder together yield the amount of plastically deformed binder per unit area of fracture surface. The volume of deformed binder and its *in situ* yield strength were combined to obtain a term proportional to the amount of plastic work done per unit area of fracture surface. It is shown that the correlation between this plastic work term and the fracture toughness of the cermets is good, while correlation with binder mean free path alone is poor.

1. Introduction

The unusual combination of high hardness and fracture toughness of WC–Co cermets has made them indispensable to a variety of engineering applications. Attempts to develop alternate cermet systems with superior performance, as measured by the hardness–fracture toughness combination, have not been very successful. A lack of complete understanding of all the factors that determine flow and fracture in this class of materials is the principal limitation. Identification and quantification of the dominant fracture mode in these materials can contribute significantly to understanding the influence of microstructural and chemical variables on the fracture behaviour of these materials and enhance the possibility of developing other superior cermet systems. Since fracture events in these materials occur at a very fine scale as dictated by the microstructure, (carbide grain size ~ 1 to $5\,\mu m$ and binder mean free path ~ 0.1 to $1\,\mu m$) quantification of the fracture mode using conventional techniques such as lineal analysis is not always reliable. This problem can be overcome through the use of a surface sensitive tool such as Auger electron spectroscopy (AES).

AES is well suited to quantitative determination of fracture modes in this class of materials due to its surface sensitivity and the limited solubility of the binder in the hard phase. In a prior investigation, Viswanadham and Sun [1] were able to determine the dominant fracture mode in VC–Ni cermets using AES. The binder/carbide ratios on polished and fracture surfaces were used to calculate a deviation parameter for the binder, Δ, defined as

$$\Delta = \left(\frac{\text{Binder/Carbide ratio on fracture surface}}{\text{Binder/Carbide ratio on polished surface}}\right) - 1. \quad (1)$$

It was shown that the deviation parameter for the binder in VC–Ni cermets can be altered from a positive to a negative value by altering the carbon-to-metal ratio and/or microstructural variables. It was also demonstrated that materials with a positive deviation parameter exhibited a hard-

0022–2461/81/041029–10$03.00/0

TABLE I Microstructural parameters for WC–Co alloys used in the study

Sample number	w_B	f_B	d_c (μm)	G	λ (μm)	λ^G (μm)
19B	0.105	0.172	1.8	0.33	0.37	0.55
19C	0.079	0.133	2.5	0.40	0.38	0.63
19D	0.057	0.093	4.5	0.50	0.46	0.92
21B	0.138	0.220	1.8	0.26	0.51	0.69
21C	0.122	0.197	2.5	0.29	0.61	0.86
21D	0.102	0.167	3.8	0.33	0.76	1.13

ness–fracture toughness combination that was superior to those with either a zero or a negative deviation parameter. A single WC–Co composition was also included in the study and showed a very high positive deviation parameter for the binder.

In this study an attempt was made to extend the earlier investigation of Viswanadham and Sun [1] to quantitatively determine the amount of binder per unit area of fracture surface in WC–Co cermets. The area fraction of binder on the fracture surface was calculated from the volume fraction of binder in the sample, and the binder/carbide ratios measured by AES on the polished and fracture surfaces. To determine the influence of changes in carbide grain size and binder content on the area fraction occupied by the binder on the fracture surface, a series of six WC–Co cermets were examined. The area fraction of binder on the fracture surface when combined with the average binder mean free path yields the volume of "heavily" deformed binder per unit area of fracture surface. Finally a fracture toughness–microstructure correlation was attempted from a knowledge of the *in situ* yield strength of the binder and the volume of deformed binder. The correlation was found to be good.

2. Materials

The relevant microstructural parameters of the WC–Co cermets used in this investigation are listed in Table I. All materials were processed by conventional powder metallurgy techniques and liquid-phase sintered in vacuum. The microstructure was pore free (A-1 ASTM rating) and reasonably uniform. Prior to testing all materials were hot isostatically pressed in argon at 1285° C and ~ 103 MPa. The weight fraction (w_B) and volume fraction (f_B) of binder were obtained from density measurements. The contiguity factor (G) was obtained by interpolation from the data of Lee and Gurland [2]. The binder mean free path (λ) and the contiguous mean free path (λ^G) were calculated from the following equations [2]:

$$\lambda = \left(\frac{f_B}{(1-f_B)}\right) \cdot \bar{d}_c \qquad (2)$$

and

$$\lambda^G = \left(\frac{f_B}{(1-f_B)}\right) \cdot \left(\frac{\bar{d}_c}{(1-G)}\right), \qquad (3)$$

where $\bar{d}_c$ is the average carbide grain size.

3. Quantitative fractography by AES

The fracture surfaces used in this investigation were obtained from the broken halves of "short-rod" fracture toughness samples [3] fractured in a servohydraulic testing sytem under ambient conditions. In this investigation the dimensional tolerances on the sample and the saw cuts were improved to decrease data scatter and obtain more reliable data [4]. All the fracture surfaces were examined in a scanning electron microscope (SEM) and secondary electron images were obtained. Typical fractographs are shown in Fig. 1a to d. The features observed on all the fracture surfaces are qualitatively very similar. The binder in all cases has failed by ductile rupture; carbide cleavage and secondary cracking are minimal. However, quantitative determination of the amount of the two phases present on the fracture surface is not possible from the SEM images alone and a surface sensitive tool such as AES has to be used.

3.1. Sample preparation for AES

Thin sections ~ 1 mm thick were cut from the broken halves of each "short-rod" specimen. The cuts were made using a diamond saw ~ 0.4 mm thick and 127 mm in diameter at 800 rpm. It was necessary to use a fluid medium during the cutting operation to prevent debris from falling on the fracture surface, as would happen during a dry cut. Water, when used as a cutting fluid reacted with the fracture surface and produced visible

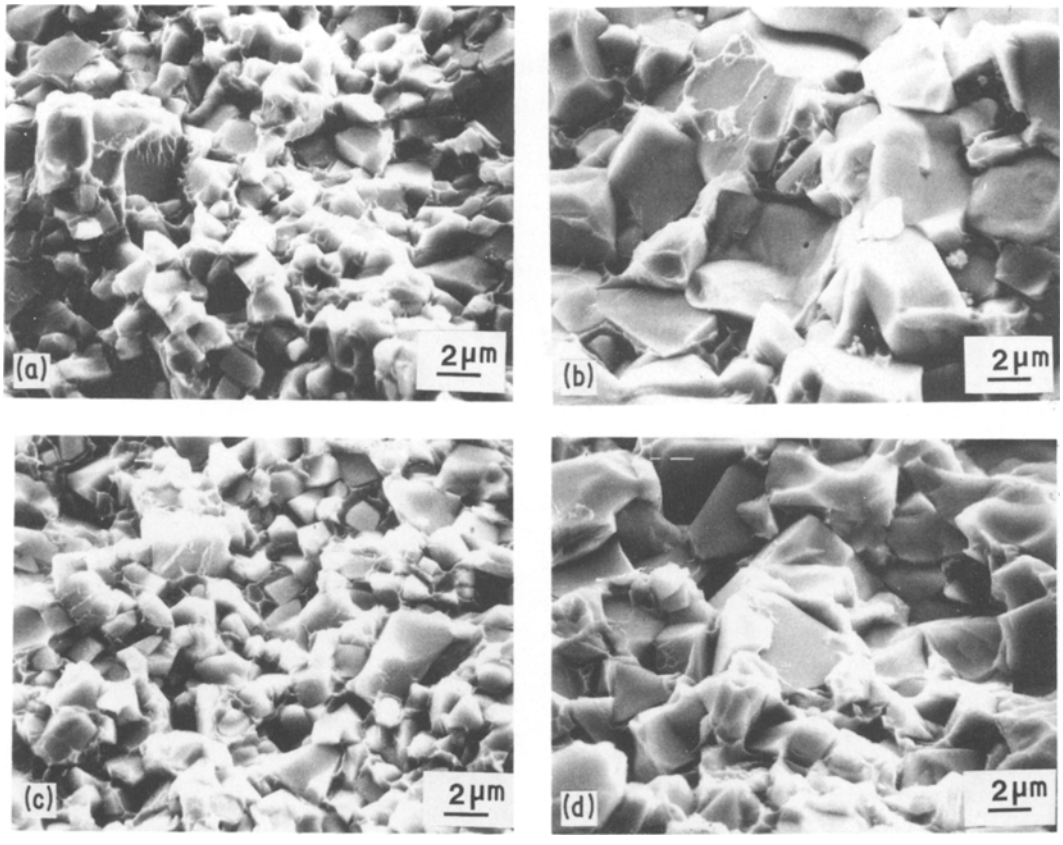

Figure 1 Scanning electron micrographs of the fracture surfaces of samples (a) 19B, (b) 19D, (c) 21B and (d) 21D.

discolouration. To avoid any reaction with the fracture surface, a kerosene base cutting fluid was used.

To prevent any mechanical damage to the fracture surface, the final cut transverse to the axis of the cylinder was prevented from going to completion and the thin section with the fractured area was removed by fracturing the uncut portion (Fig. 2). The thin section containing the fracture surface was then transferred to a methanol bath with the fracture surface facing upwards, ultrasonically cleaned, air dried and individually stored in sealed plastic bags. The thin section

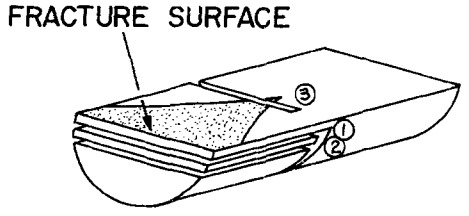

(a) SHORT-ROD BROKEN HALF CUTS ①, ② AND ③

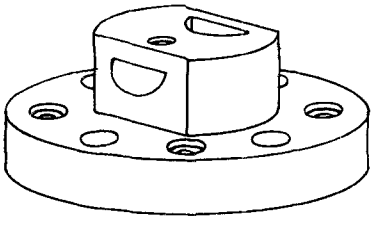

(b) SPECIMEN HOLDING FIXTURE

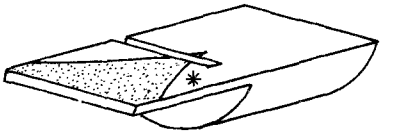

*HELD HERE AND BROKEN WHILE IN THE FIXTURE

(c) RETRIEVAL OF THIN SECTION WITH FRACTURE SURFACE

Figure 2 Schematic illustration of the specimen fixture and the saw cuts used to prepare samples for Auger spectroscopy.

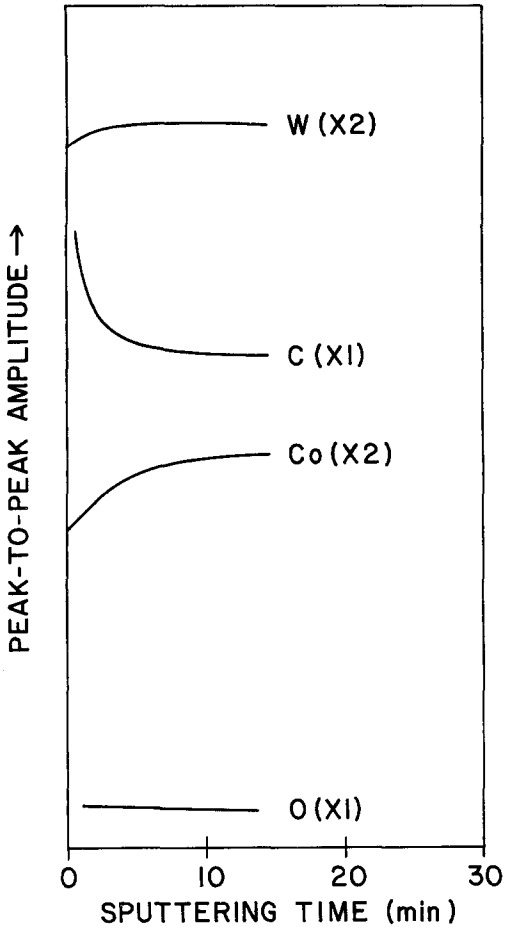

Figure 3 Variation in the peak-to-peak amplitudes of Co, W, C and O during sputtering of a polished sample.

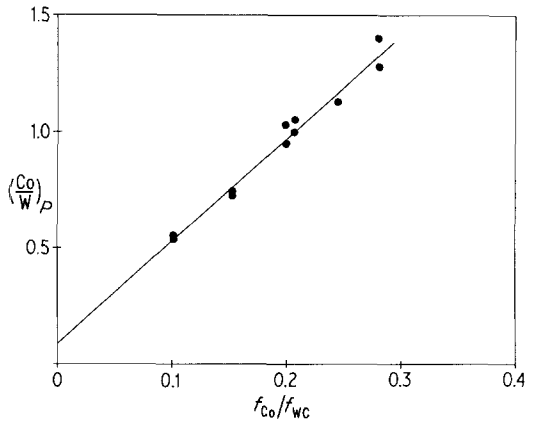

Figure 4 (Co/W) peak-to-peak height ratios measured on polished samples plotted against the ratio of bulk volume fractions of binder and carbide.

adjacent to the one containing the fracture surface was metallographically polished with successively finer diamond paste and finished with ~1 μm grit.

3.2. Auger spectroscopy

The (Co/W) ratios determined on both polished and fracture surfaces in the as-received condition were influenced by the presence of oxides (fracture surfaces) and hydrocarbon contamination (polished surfaces). To remove the contamination, the surfaces were sputtered with an argon ion beam at 2 keV and 50 μA cm^{-2} ion current. The sputtered area was ~3 mm in diameter and the analysed area ~0.5 mm in diameter. The behaviour of the following peaks was monitored during sputtering: The Co : $L_3M_{4,5}M_{4,5}$ peak at 775 eV, the W : $M_5N_7N_7$ peak at 1736 eV, the oxygen : KL_2L_2 peak at 510 eV and the C : KL_2L_2 peak at 272 eV. In the polished samples the oxygen peak was reduced to negligible values within ~1 min of sputtering and all the other peaks reached saturation values within ~5 min of sputtering. Typical behaviour of the peak-to-peak heights (PPH) during sputtering of a polished sample is shown in Fig. 3. The (Co/W) ratios were obtained from the saturation values of the PPH's of Co and W. When the (Co/W) ratios measured by AES are plotted against the ratio of bulk volume fractions of binder and carbide present in the sample, a linear plot was obtained (Fig. 4) indicating no significant preferential sputtering of cobalt. The small non-zero intercept on the ordinate is most probably due to data scatter or errors in measurement of f_B and/or (Co/W) ratio at low volume fractions. If the plot was forced to go through the origin the correlation coefficient was not significantly reduced.

The behaviour of the peak-to-peak amplitudes during sputtering of a fracture surface is shown in Fig. 5. The cobalt PPH increased and reached a maximum value within 2 to 3 min of sputtering. At about the same time the oxygen peak was reduced to very low values and the carbon peak began to saturate. This behaviour was observed on all the fracture surfaces examined with the exception of those that reacted with water. The reacted fracture surfaces were covered with cobalt oxides and hydroxides and no tungsten was observed in the as-received condition.

Continued sputtering led to a decrease in the cobalt PPH and an increase in the tungsten PPH. The continuous nature of these changes implies that not all the cobalt on the fracture surface was

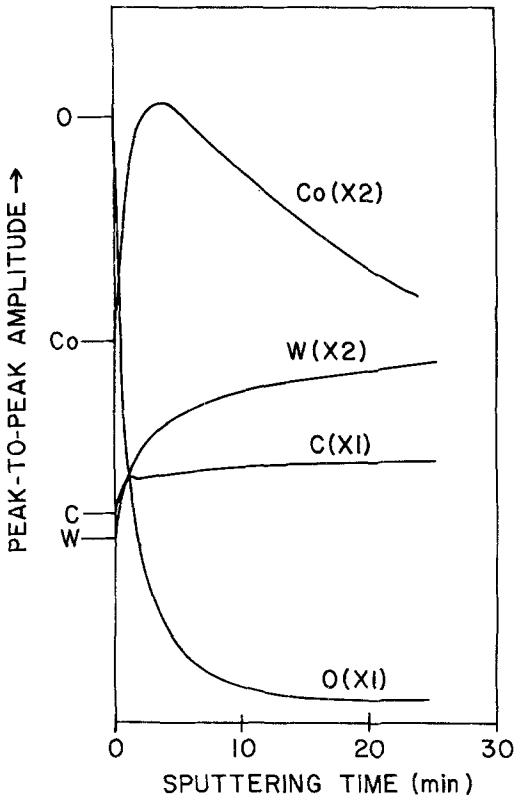

Figure 5 Variation in the peak-to-peak amplitudes of Co, W, C and O during sputtering of a fracture surface.

of uniform thickness and removal of the thinner cobalt areas would continuously expose underlying carbide and result in an increase in the tungsten signal. However, the saturation behaviour of carbon was an anomaly and no satisfactory explanation could be found.

The (Co/W) ratios for the fracture surfaces were obtained from the PPH ratio of cobalt and tungsten at the point where the cobalt was a maximum. This procedure was justified because cobalt was the component that reacted more readily with any moisture or oxygen upon exposure of the fracture surface to the ambient atmosphere and the cobalt signal in the as-received condition will not be representative of the true amount. Secondly, the cobalt PPH reached a maximum at about the same time as the oxygen peak was reduced to very low values, indicating removal of a thin layer of cobalt oxide from the as-received fracture surface. (Co/W) ratios calculated this way were reproducible on mating surfaces and duplicate samples from the same group while (Co/W) ratio calculated from the PPH values in the as-received condition were not.

3.3. Area fraction occupied by the binder on the fracture surface

If the assumption is made that the small non-zero intercept on the ordinate in Fig. 4 is due to experimental scatter, and the (Co/W) ratio measured on a polished section, $(Co/W)_p$, is proportional to the ratio of binder and carbide volume fractions present in the bulk, then

$$\left(\frac{Co}{W}\right) = k\,(f_B/f_c), \tag{4}$$

where k is a constant of proportionality that includes the relative Auger sensitivities etc. If the same proportionality is assumed to hold for the fracture surfaces, then the (Co/W) ratio measured on fracture surfaces, $(Co/W)_f$, can be written as

$$\left(\frac{Co}{W}\right)_f = k\left(\frac{A_f^{Co}}{1 - A_f^{Co}}\right), \tag{5}$$

where A_f^{Co} is the area fraction of binder on the fracture surface. Rearranging Equation 5

$$A_f^{Co} = (Co/W)_f/[(Co/W)_f + k]. \tag{6}$$

Substituting from Equation 4

$$A_f^{Co} = \left(\frac{Co}{W}\right)_f \Big/ \left[\left(\frac{Co}{W}\right)_f + \left(\frac{Co}{W}\right)_p \left(\frac{f_c}{f_B}\right)\right]. \tag{7}$$

The (Co/W) ratios measured on polished and fracture surfaces and average values for area fraction of binder on the fracture surface obtained from Equation 7 are listed in Table II. Although the overall range in binder content and carbide grain size of the samples examined is limited, certain trends in A_f^{Co} with changes in both of these microstructural parameters are apparent. A_f^{Co} increases with increase in binder content and decreases with increase in carbide grain size. The decrease in A_f^{Co} with increase in carbide grain size is more noticeable at lower binder contents (compare the two groups 19 and 21 in Table II).

4. Fracture toughness

4.1. Fracture toughness measurements

The plane-strain fracture toughness (K_{IC}) of the cermets used in this investigation was obtained from samples of the "short-rod" geometry [3]. In this geometry a cylindrical sample ~ 12.7 mm diameter and ~ 18.8 mm high was notched with a diamond saw, as shown in Fig. 6. The crack was started at the tip of the uncut region and propagates stably at first and then becomes unstable. The position where the crack becomes unstable bears an

TABLE II (Co/W) ratios measured on the polished and fracture surfaces of the cermets listed in Table I. The average area fraction of binder on the fracture surface was obtained from Equation 7

Sample number	Comments	$\left(\frac{C}{W}\right)_P$	$\left(\frac{Co}{W}\right)_P$	$\left(\frac{Co}{W}\right)_f$	A_f^{Co} (Average)
19B		1.35	1.05	3.80	0.44
19B		1.31	1.00	4.11	
19C		1.32	0.74	2.89	0.37
19C		1.37	0.73	2.84	
19D		1.35	0.55	2.16	
19D	Mating fracture surface	—	—	2.22	0.29
19D		1.37	0.54	2.09	
21B		1.29	1.28	4.22	
21B	Reacted with H_2O. No W signal	1.29	1.40	—	0.47
21C		1.37	1.13	3.58	0.44
21D		1.36	1.03	3.02	
21D	Reached with H_2O. No W signal	1.36	0.95	—	0.38

invariant relationship to the sample geometry [3]. Based on this observation it was possible to obtain K_{IC} from the peak load and a compliance calibration factor.

In a recent investigation of fatigue properties of WC–Ni composites, Drake [4] has shown that by stringent control of the sample geometry, cut width and location, random errors can be reduced to very low values and K_{IC} values can be obtained to within ± 0.8%. This was verified on a statistical sample of 50 nominally identical WC–Ni cermets. In the present investigation the K_{IC} values were obtained from cylinders ground and cut to the specifications established in the WC–Ni study [4].

The plane-strain fracture toughness values measured on the samples listed in Table I are shown in Table III. The Young's modulus (E) and Poisson's ratio (ν) were taken from the data of Doi *et al.* [5].

4.2. Correlations with microstructural parameters

Various attempts have been made over the years to develop correlations between the fracture toughness of WC–Co cermets and their microstructure [6–14]. In most instances the effect of variations in carbide grain size and binder content on fracture toughness is expressed through their influence on binder mean free path and a linear relationship is predicted between the critical strain energy release rate (G_{IC}) and the binder mean free path [9]. However, our attempts to do

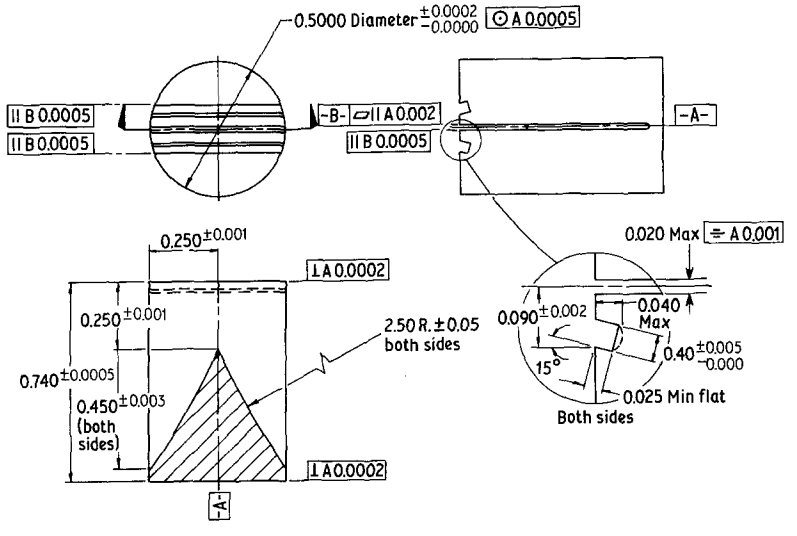

Figure 6 The "short-rod" sample geometry and the tolerances used for measuring K_{IC} of WC–Co cermets.

TABLE III Fracture toughness of WC–Co cermets used in the study

Sample number	K_{IC} (MPa $(m^{1/2})$)	E (GPa)	ν	G_{IC} ($J\,m^{-2}$)
19B	14.26	576.6	0.21	337
19C	14.09	600.2	0.21	316
19D	14.92	627.6	0.21	339
21B	15.36	545.2	0.21	414
21C	16.41	560.9	0.21	459
21D	17.11	580.6	0.21	482

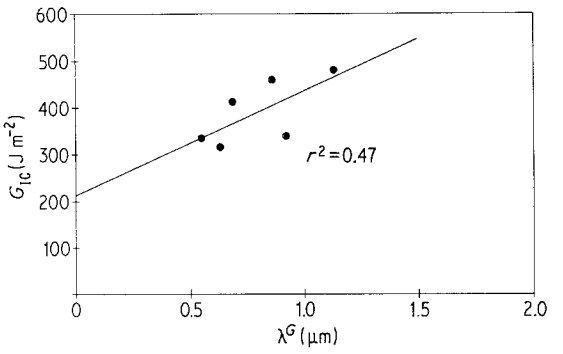

Figure 7 Measured fracture toughness G_{IC} plotted against the contiguous mean free path λ^G. The correlation is poor.

so resulted in poor correlation (Fig. 7). Although the contiguous binder mean free path, λ^G, was used in this instance, the correlation is equally poor even if the nominal binder mean free path was used. To verify whether this poor correlation was peculiar to our results, data available on fracture toughness of WC–Co cermets from a variety of different sources [6–17] were compiled and plotted against the contiguous binder mean free path, λ^G. To obtain this compilation, the following assumptions were made:

(a) All fracture toughness measurement techniques are of equal validity;

(b) Carbide grain size and binder content can be measured more accurately than binder mean free path;

(c) Contiguity is a function of binder content only.

The contiguity values were obtained by interpolation from the data of Lee and Gurland [2]. The contiguity, carbide grain size and binder content were combined to yield the contiguous mean free path, λ^G (Equation 2). Where necessary the Young's Modulus and Poisson's ratio were interpolated from the results of Doi *et al.* [5]. The compilation is shown in Fig. 8. Any attempt to fit all the data to a single linear function results in poor correlation. If the compilation is divided into two groups (somewhat arbitrarily), those with carbide grain sizes $\leqslant 1.5\,\mu m$ and those with carbide grain sizes $\geqslant 3\,\mu m$, certain trends begin to emerge. The G_{IC} data at small grain sizes show excellent linear correlation with λ^G. The data for large grain samples exhibit considerable scatter and the correlation is poor. Since the grain size of the cermets used in our investigation roughly spans these two ranges, the overall correlation between G_{IC} and λ^G is poor. Interestingly enough, if only Samples 19B and 21B are considered ("small" grain) the correlation is considerably improved.

This exercise serves to show that to develop fracture toughness–microstructure correlations in WC–Co, factors other than the binder mean free path need to be taken into account. Two factors that come to mind are the extent of various fracture modes and the specific stress–strain response of the binder phase. Some attempts along these lines have already been undertaken. For

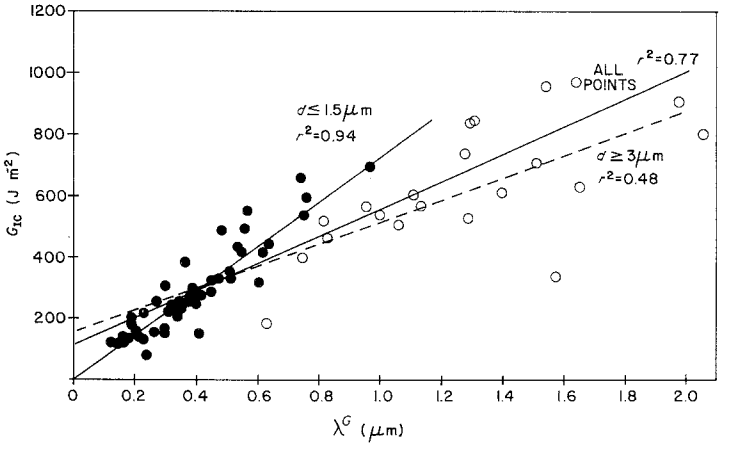

Figure 8 Compilation of fracture toughness data available on WC–Co cermets plotted against the contiguous mean free path λ^G. The correlation is good only when the carbide grain size is $\leqslant 1.5\,\mu m$.

example, Pickens and Gurland [10] developed a model for the fracture toughness of WC–Co alloys based on the Rice–Johnson ductile–fracture criterion [18] and obtained a relationship of the form

$$\sigma_y \lambda = \alpha G_{IC}, \quad (8)$$

where σ_y is the yield strength of the unbroken ligaments and α is a constant. σ_y was derived from indentation hardness measurements. Murray [9] developed a model where the binder was assumed to deform at its theoretical shear strength. However, dislocation structures observed in the binder phase in deformed WC–Co cermets [19] invalidate this view and indicate instead that the binder deforms by dislocation generation, motion and interaction; subject of course to the constraint and the strong image forces imposed by the presence of carbide grains in close proximity. Also, fractographs obtained on WC–Co cermets show that the binder fractures by void nucleation, growth and coalescence; features not usually attributable to failure at theoretical shear strength. Irrespective of the specific assumption about the stress–strain response of the binder, all fracture toughness–microstructure models developed to date lack detailed quantitative information on fracture modes and the exent of the two phases present on the fracture surface. Since this information is now available through Auger spectroscopy, an attempt will be made to develop a fracture toughness–microstructure models developed so far lack ating the quantitative information on the fracture surfaces obtained by AES.

4.3. Current model

In the current model, analogous to those developed earlier [11, 12], it is assumed that the energy expended in the flow and fracture of the binder is the single most dominant factor in determining fracture toughness of the cermets. Surface energy terms and all other fracture modes are ignored. The critical strain energy release rate (G_{IC}) can then be written as [20].

$G_{IC} = \alpha$ (volume of deformed binder/unit area of fracture surface) × (plastic work) done per unit volume of deformed binder),

where α is a constant.

The volume of deformed binder can be written to a first approximation as $A_f^{Co}\lambda^G$. The plastic work done on the binder per unit volume can be written as $\int_0^{\epsilon_f} \sigma_B(\epsilon)\, d\epsilon$ up to a fracture strain, ϵ_f.

To evaluate the plastic work term detailed knowledge of the stress–strain behaviour of the binder phase is required. This is not known, particularly when the stress field is tensile. Lindau [21] has shown that the compressive yield strength of a variety of WC–Co alloys can be described by a single function if the binder flow strength can be written as

$$\sigma_y^B = \sigma_y^o + k[\lambda^G]^{-1/2}, \quad (9)$$

where σ_y^o is the yield strength of the binder in bulk and k is a Hall–Petch constant. Relationships with similar functional forms have been proposed by other authors [2, 22]. Lindau analysed the compressive flow strength data of both Doi *et al.* [23] and Johansson and Gustavsson [24] and arrived at slightly different values for σ_y^o and k. The flow strength obtained from the data of Johansson and Gustavsson is considered to be more reliable due to the care exercised in preventing end-effects during testing. Lindau derived the following relationship for the flow strength of the binder from Johansson and Gustavsson's data

$$\sigma_y^B = 480 + 7.7[\lambda^G]^{-1/2}\,\mathrm{N\,mm^{-2}}. \quad (10)$$

Depending on the flow strength data selected (0.2 or 0.5%) for the composite, different values can be arrived at for σ_y^B and k. However, the functional form will remain the same. Although the above expression describes only the compressive flow strength of the binder, it will be assumed that tensile flow strength can also be described by the same function. The work hardening behaviour and the fracture strain of the binder are unknown. The fracture surfaces of all the WC–Co cermets examined show that the binder in all cases fractures by ductile rupture. Except for local variations in dimple size etc. present in any sample, the final ligament sizes and shapes in all the cermets are surprisingly similar. This implies that the fracture strain and the work hardening behaviour of the binder among the cermets examined were not drastically different. If the fracture strain is assumed to be ϵ_f in all cases and the binder is modeled as a rigid plastic material, the plastic work done per unit volume of deformed binder can be written as

$$\text{plastic work} \simeq \sigma_y^B \epsilon_f.$$

The fracture toughness (G_{IC}) becomes

$$G_{IC} \simeq \alpha \sigma_y^B \epsilon_f A_f^{Co} \lambda^G. \quad (11)$$

TABLE IV Volume of deformed cobalt per unit area of fracture surface, the calculated *in situ* yield strength of the binder phase and their product

Sample number	λ^G (μm)	A_f^{Co}	$A_f^{Co}\,\lambda^G$ ($\times 10^6$ m^3)	σ_y^B (MPa)	$\sigma_y^B\,A_f^{Co}\,\lambda^G$ (J m^{-2})
19B	0.55	0.44	0.242	808.3	195.6
19C	0.63	0.37	0.233	786.3	183.2
19D	0.92	0.29	0.267	733.9	196.0
21B	0.69	0.47	0.324	773.1	250.5
21C	0.86	0.44	0.378	742.6	280.7
21D	1.13	0.38	0.429	709.1	304.2

The calculated σ_y^B values and the volume of deformed binder per unit area of fracture surface, ($A_f^{Co}\,\lambda^G$), are listed in Table IV. A plot of G_{IC} against $\sigma_y^B\,A_f^{Co}\,\lambda^G$ is shown in Fig. 9 and the correlation is very good.

As previously discussed, A_f^{Co} is sensitive to variations in binder content and carbide grain size. This implies that microstructural variables exert their influence on fracture toughness not only through variations in binder mean free path but also through changes in A_f^{Co}. This can result in a dual effect on fracture toughness. For example, if the carbide grain size for a fixed binder content is increased λ^G will increase (a higher G_{IC}) and A_f^{Co} will decrease (a lower G_{IC}). In the range of grain sizes used in this study, the effect on λ^G is dominant and the fracture toughness increases. However, if the grain size is further increased, a point can be reached where the two effects cancel each other. Since the decrease in A_f^{Co} with increase in grain size is more rapid at low binder contents, the dual effect of grain size will be easily noticeable and increases in fracture toughness will not keep pace with increases in λ^G.

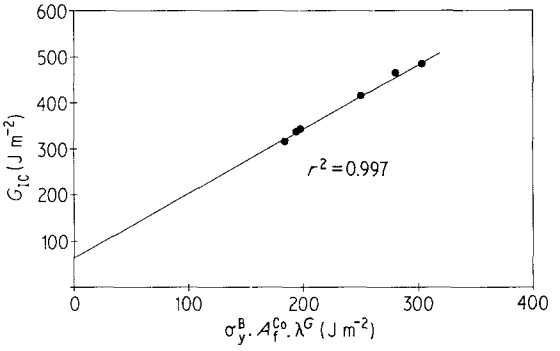

Figure 9 A plot of measured fracture toughness G_{IC} in J m^{-2} against the product $\sigma_y^B\,A_f^{Co}\,\lambda^G$ where σ_y^B is the *in situ* binder yield strength, A_f^{Co} is area fraction of binder on the fracture surface and λ^G is the binder mean free path. The correlation is good.

5. Conclusions

Auger electron spectroscopy (AES) has been shown to be a very useful tool for quantitative fractography of cemented carbide systems. A general procedure has been described whereby quantitative information in the form of area fraction of binder on fracture surfaces can be obtained. The area fraction of binder on the fracture surface (A_f^{Co}) is sensitive to microstructural parameters such as carbide grain size and binder content. It increases with increase in binder content and decreases as the carbide grain size is increased. Microstructural variables influence fracture toughness not only through their effect on binder mean free path, but also through their effect on A_f^{Co}. The binder mean free path, the area fraction of binder on the fracture surface, and the *in situ* yield behaviour of the binder are the three principal factors that determine fracture toughness in these materials. Attempts to correlate fracture toughness with binder mean free path alone were not successful.

Acknowledgements

The able assistance of Mr H. B. Pratt and G. Morgan in preparation of the samples and thin sections and the assistance of Mr R. Butler in obtaining the Auger spectra is gratefully acknowledged. The authors also wish to express their thanks to Mrs R. Robinson for her patient and skillful assistance in the preparation of this manuscript.

References

1. R. K. VISWANADHAM and T. S. SUN, *Scripta Met.* **13** (1977) 767.
2. H. C. LEE and J. GURLAND, *Mater. Sci. Eng.* **33** (1978) 125.
3. L. M. BARKER, *Eng. Fract. Mech.* 9 (1977) 361.
4. E. F. DRAKE, PhD. dissertation, Rice University, Houston, Texas, 1980.
5. H. DOI, Y. FJUIWARA, K. MIYAKE and Y. OOSAWA, *Met. Trans.* **1** (1970) 1417.

6. N. INGELSTROM and H. NORDBERG, *Eng. Fract. Mech.* **6** (1974) 597.
7. R. C. LUETH, "Fracture Mechanics of Ceramics", Vol. 2, edited by R. C. Bradt, D. P. H. Hasselmann and F. F. Lange (Plenum Press, New York and London, 1974) p. 791.
8. J. L. CHERMANT and F. OSTERSTOCK, *J. Mater. Sci.* **11** (1976) 1939.
9. M. J. MURRAY, *Proc. Roy. Soc. A.* **356** (1977) 483.
10. J. R. PICKENS and J. GURLAND, *Mater. Sci. Eng.* **33** (1978) 135.
11. L. LINDAU, "Fracture", Proceedings of the Fourth International Conference on Fracture Vol. 2, Waterloo, Canada, (1977) p. 21.
12. T. JOHANNESSON, Fourth European Symposium on Powder Metallurgy, Paper No. 5-11-1, Grenoble, France, 1975.
13. C. CHATFIELD, The Fifth European Symposium on Powder Metallurgy, Vol. 2 (Jernkontoret, Stockholm, Sweden, 1978) p. 57.
14. M. NAKAMURA and J. GURLAND, *Met. Trans. A.* **11A** (1980) 141.
15. E. A. ALMOND and B. ROEBUCK, *Met. Tech.* **5** (1978) 92.
16. C. M. PERROTT, *Wear* **47** (1978) 81.
17. M. J. MURRAY and C. M. PERROTT, "Advances in Hard Material Tool Technology", edited by R. Komanduri, (Carnegie Press, Pittsburgh, Pa. 1976) p. 314.
18. J. R. RICE and M. A. JOHNSON, "Inelastic Behaviour of Solids", edited by M. Kanninen, W. Adler, W. Rosenfield and R. Jaffe (McGraw Hill, New York, 1974) p. 641.
19. V. K. SARIN and T. JOHANNESSON, *Met. Sci.* 9 (1975) 472.
20. J. P. HIRTH and F. H. FROES, *Met. Trans. A* **8A** (1977) 1165.
21. L. LINDAU, *Scand. J. Met.* **6** (1977) 90.
22. J. L. CHERMANT and F. OSTERSTOCK, *Powder Met. Int.* **11** (1979) 106.
23. H. DOI, Y. FUJIWARA and K. MIYAKE, *Trans. AIME* **245** (1969) 1457.
24. I. JOHANSSON and L. E. GUSTAVSSON, Sandvik Coromant Lab, Report No. 2246 (referenced in [11]).

Received 14 April and accepted 3 October 1980.